# Atomic-scale computer simulation for early precipitation process of $Ni_{75}Al_{10}V_{15}$ alloy*

ZHAO Yuhong**, CHEN Zheng, WANG Yongxin and LU Yanli

(Department of Materials Science and Engineering, Northwestern Polytechnical University, Xi'an 710072, China)

Received May 21, 2003; revised June 15, 2003

**Abstract** The kinetic model for a ternary system is introduced based on the microscopic diffusion form of the phase-field equations for a binary alloy. The equation is solved in the reciprocal space. This model is used to investigate the early precipitation process of $Ni_{75}Al_{10}V_{15}$ by simulating the atomic pictures of the two ordered phases and calculating the order parameters of $\gamma'$ ($Ni_3Al$) phase. Simulation results show that the $\gamma'$ ordered phases precipitate from the disordered matrix by a non-classical nucleation mechanism, and the nonstoichiometric $\gamma'$ ordered phase appears first and then transforms into the stoichiometric one. Clusters of V atoms appear at the $\gamma'$ phase boundaries followed by the formation of the nonstoichiometric $\theta$ ordered phase. The farther the location from $\gamma'$ phase boundary is, the lower the order degree of $\theta$ phase is. There exist two kinds of $DO_{22}$ ordered domains: a horizontal one and a vertical one, related to their adjacent $\gamma'$ phase boundaries. The model could describe the atomic ordering and composition clustering simultaneously, and any a priori assumption about the new phase structure and precipitation mechanism etc. is unnecessary.

**Keywords:** early precipitation process, computer simulation, $Ni_{75}Al_{10}V_{15}$ alloy.

Since the study of the microstructure formation in alloy is one of the most important research subjects in the materials science, a great deal of experimental work has been carried out. However, the theoretical study of the inevitability of microstructure formation has hardly been conducted, because the microstructure is diversified for each alloy[1]. Recently, the non-linear dynamics of pattern formation has remarkably developed on the basis of computational investigation, and four methods have mainly been used, i.e. (1) Monte-Carlo model, (2) molecular dynamics, (3) master equation and (4) phase-field model[2].

The phase-field method has recently emerged as a powerful computational approach to modeling and predicting mesoscale morphological and microstructure evolution in materials. In this paper, the microscopic diffuse form of the phase-field equation for a binary system is extended to a ternary system. With the fast Fourier transform and projection relationship, the 3D non-linear partial derivative equation in the real space is transformed to a 2D linear constant derivative equation in the reciprocal space. So, the calculation work has been decreased dramatically. This model does not need any a priori assumption about the new phase microstructure and precipitation mechanism, and does not define or separate the precipitation process. It can simultaneously describe atomic ordering and composition clustering so as to present a theoretical basis for designing aging procedures on atomic scale.

## 1 Phase-field model for precipitation kinetics

It describes a microstructure using a set of conserved and nonconserved field variables that are continuous across the interfacial regions[3]. For a binary alloy, the composition and structural differences between the two phases are described by a conserved field variable $c(\boldsymbol{r})$ and a non-conserved field $\eta(\boldsymbol{r})$ variable[4~6]. The evolution of field variables can be obtained by solving the following Cahn-Hilliard and Allen-Cahn equations[6]:

$$\frac{\partial c(\boldsymbol{r}, t)}{\partial t} = M \nabla^2 \frac{\partial F}{\partial c(\boldsymbol{r}, t)}, \tag{1a}$$

$$\frac{\partial \eta_p(\boldsymbol{r}, t)}{\partial t} = -L \frac{\partial F}{\partial \eta_p(\boldsymbol{r})}; \quad p = 1, 2, 3\cdots, \tag{1b}$$

where $M$ and $L$ are related to the solute atom mobility, and $p$ stands for structural order parameters of different orientations.

Since our work does not concern the change in

* Supported by the National Natural Science Foundation of China (Grant No. 50071046)

** To whom correspondence should be addressed. E-mail: zyh388@sina.com

lattice structure, Eq. (1a) can describe the isostructural transformation and (1b) becomes unnecessary here. For a binary substituted alloy, the microscopic discrete lattice form of (1a) is given by[7]:

$$\frac{\mathrm{d}P(\boldsymbol{r},t)}{\mathrm{d}t}=\frac{C_0(1-C_0)}{k_{\mathrm{B}}T}\sum_{\boldsymbol{r}'}L(\boldsymbol{r}-\boldsymbol{r}')\frac{\partial F}{\partial P(\boldsymbol{r},t)}, \tag{2}$$

where the function $P(\boldsymbol{r},t)$ characterizes a single site occupation probability on the site $\boldsymbol{r}$ at time $t$, which describes the morphology of precipitate; $L(\boldsymbol{r}-\boldsymbol{r}')$ is a constant matrix related to probabilities of elementary diffusion jumps from lattice $\boldsymbol{r}$ to $\boldsymbol{r}'$; $T$ the absolute temperature; $k_{\mathrm{B}}$ the Boltzmann's constant; $C_0$ the average alloy composition; and $F$ the total free energy of the system.

For a ternary system, the atomic configurations and the phase morphologies are described by the single-site occupation probability functions $P_{\mathrm{A}}(\boldsymbol{r},t)$, $P_{\mathrm{B}}(\boldsymbol{r},t)$ and $P_{\mathrm{C}}(\boldsymbol{r},t)$, which represent the probabilities of finding an A, B and C at a given lattice site $\boldsymbol{r}$ at a given time $t$. Since $P_{\mathrm{A}}(\boldsymbol{r},t)+P_{\mathrm{B}}(\boldsymbol{r},t)+P_{\mathrm{C}}(\boldsymbol{r},t)=1$, only two equations are independent at each lattice site. Assuming the independent variables are $P_{\mathrm{A}}(\boldsymbol{r},t)$ and $P_{\mathrm{B}}(\boldsymbol{r},t)$, we can write the microscopic diffusion equations for a ternary system as

$$\begin{cases}\dfrac{\mathrm{d}P_{\mathrm{A}}(\boldsymbol{r},t)}{\mathrm{d}t}=\dfrac{1}{k_{\mathrm{B}}T}\sum\limits_{\boldsymbol{r}'}\Big[L_{\mathrm{AA}}(\boldsymbol{r}-\boldsymbol{r}')\dfrac{\partial F}{\partial P_{\mathrm{A}}(\boldsymbol{r}',t)}\\ \qquad +L_{\mathrm{AB}}(\boldsymbol{r}-\boldsymbol{r}')\dfrac{\partial F}{\partial P_{\mathrm{B}}(\boldsymbol{r}',t)}\Big]\\ \dfrac{\mathrm{d}P_{\mathrm{B}}(\boldsymbol{r},t)}{\mathrm{d}t}=\dfrac{1}{k_{\mathrm{B}}T}\sum\limits_{\boldsymbol{r}'}\Big[L_{\mathrm{BA}}(\boldsymbol{r}-\boldsymbol{r}')\dfrac{\partial F}{\partial P_{\mathrm{A}}(\boldsymbol{r}',t)}\\ \qquad +L_{\mathrm{BB}}(\boldsymbol{r}-\boldsymbol{r}')\dfrac{\partial F}{\partial P_{\mathrm{B}}(\boldsymbol{r}',t)}\Big],\end{cases} \tag{3}$$

where $L_{\alpha\beta}(\boldsymbol{r}-\boldsymbol{r}')$ are the exchange probabilities between a pair of atoms $\alpha$ and $\beta$ at lattice sites $\boldsymbol{r}$ and $\boldsymbol{r}'$ per unit time, $\alpha,\beta=\mathrm{A,B,C}$.

In the single-site approximation, the non-equilibrium free energy $F$ for a ternary system is given by[8,9]

$$\begin{aligned}F=&-\frac{1}{2}\sum_{\boldsymbol{r}}\sum_{\boldsymbol{r}'}[V_{\mathrm{AB}}(\boldsymbol{r}-\boldsymbol{r}')P_{\mathrm{A}}(\boldsymbol{r})P_{\mathrm{B}}(\boldsymbol{r}')\\ &+V_{\mathrm{BC}}(\boldsymbol{r}-\boldsymbol{r}')P_{\mathrm{B}}(\boldsymbol{r})P_{\mathrm{C}}(\boldsymbol{r}')\\ &+V_{\mathrm{AC}}(\boldsymbol{r}-\boldsymbol{r}')P_{\mathrm{A}}(\boldsymbol{r})P_{\mathrm{C}}(\boldsymbol{r}')]\\ &+k_{\mathrm{B}}T\sum_{\boldsymbol{r}}[P_{\mathrm{A}}(\boldsymbol{r})\ln(P_A(\boldsymbol{r}))\\ &+P_{\mathrm{B}}(\boldsymbol{r})\ln(P_{\mathrm{B}}(\boldsymbol{r}))\\ &+P_{\mathrm{C}}(\boldsymbol{r})\ln(P_{\mathrm{C}}(\boldsymbol{r}))].\end{aligned} \tag{4}$$

And

$$\begin{aligned}V_{\mathrm{AB}}(\boldsymbol{r}-\boldsymbol{r}')&=W_{\mathrm{AA}}(\boldsymbol{r}-\boldsymbol{r}')+W_{\mathrm{BB}}(\boldsymbol{r}-\boldsymbol{r}')\\ &\quad-2W_{\mathrm{AB}}(\boldsymbol{r}-\boldsymbol{r}'),\\ V_{\mathrm{BC}}(\boldsymbol{r}-\boldsymbol{r}')&=W_{\mathrm{BB}}(\boldsymbol{r}-\boldsymbol{r}')+W_{\mathrm{CC}}(\boldsymbol{r}-\boldsymbol{r}')\\ &\quad-2W_{\mathrm{BC}}(\boldsymbol{r}-\boldsymbol{r}'),\\ V_{\mathrm{AC}}(\boldsymbol{r}-\boldsymbol{r}')&=W_{\mathrm{AA}}(\boldsymbol{r}-\boldsymbol{r}')+W_{\mathrm{CC}}(\boldsymbol{r}-\boldsymbol{r}')\\ &\quad-2W_{\mathrm{AC}}(\boldsymbol{r}-\boldsymbol{r}'),\end{aligned} \tag{5}$$

in which $W_{\alpha\beta}(\boldsymbol{r}-\boldsymbol{r}')$ are the pairwise interaction energies between a pair of atoms $\alpha$ and $\beta$ at lattice sites $\boldsymbol{r}$ and $\boldsymbol{r}'$. Here a fourth-neighbor interaction model is employed.

Substituting the expression (4) into (3), using the 2D and 3D projection relationships, Fourier transforming both sides of Eq. (3), then the precipitation kinetic equation for a ternary alloy system in the reciprocal space is obtained. It is convenient and even computationally advantageous to solve the kinetic equations in the reciprocal space. The Euler method is used to solve the equations, and then the inverse Fourier transformation is carried out; finally the relationships between occupation probability and time are obtained[10].

## 2 Simulation results and discussion

The alloy system simulated is $Ni_{75}Al_{10}V_{15}$ aged at 1046.5 K. Its atomic configuration and multiphase morphologies are represented by a gray scale picture on which the black indicates 1 and the white 0. All the intermediate values are represented by different shades of gray.

Kinetic equation (3) is deterministic and hence cannot describe processes that require thermal fluctuations. Therefore, a random noise term satisfying the fluctuation-dissipation theory is introduced to promote nucleation. In this paper, the time steps added noise terms are 500.

A 2D simulation is performed in a square lattice consisting of 64×64 unit cells, and periodic boundary conditions are applied.

### 2.1 Precipitation mechanism of $\gamma'$ phase

The equilibrium $L1_2$ ordered structure diagram, its projection on [001] and its nonstoichiometric one's projection on [001] are shown in Fig. 1 (a~c). The circle's gray level represents the occupation probability of Al atom, the white is 0 and the black is 1. The corner sites are defined as B sites, others A

sites. In Fig. 1 (b), the finding probabilities of Al atoms sitting at B sites are near 1, while those sitting at A sites are near 0. In Fig. 1 (c), the finding probabilities of Al atoms at B sites are always higher than that at A sites, yet their values may be far lower than 1. We call the ordered phases satisfying this type structure nonstoichiometric ordered phases.

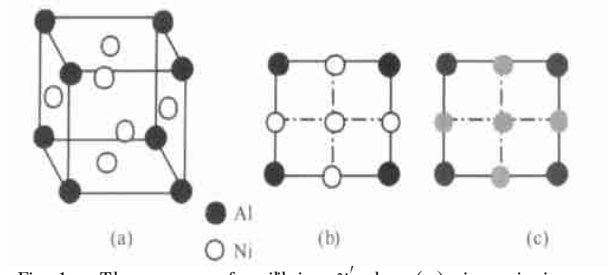


Fig. 1. The structure of equilibrium $\gamma'$ phase (a), its projection on [001] orientation (b) and nonstoichiometric $\gamma'$ ordered phase (c).

Fig. 2 (a ~ d) shows the morphological evolution of the $Ni_{75}Al_{10}V_{15}$ alloy at different time steps with the $\gamma'$ ($Ni_3Al$) phase as a main object.

The simulation results with $t = 600$ are presented in Fig. 2 (a). It can be seen that there exist composition fluctuations in the disordered matrix, and some small $L1_2$ ordered phases appear at some sites with a higher occupation probability of Al atom. The $L1_2$ ordered domains could be identified by the sites arranged in a square lattice consistent with the projection of the cubic $L1_2$ phase shown in Fig. 1. However, the occupation probabilities of Al atoms at B sites are much lower than 1, so we consider they could be nonstoichiometric ordered phases.

As shown in Fig. 2 (b), at $t = 800$, the $\gamma'$ particles are randomly distributed and its number is increasing. The interfaces between the ordered and disordered phases are diffusing with about 3-lattice sites' width, which is different from the sharp interface model in classical nucleation theory. Meanwhile, the occupation probabilities of Al atoms at B sites become higher.

In Fig. 2 (c), at $t = 1200$, the size of $\gamma'$ particles is still increasing, the occupation probabilities of Al atoms at B sites become higher, the interface width becomes narrower to about 2 sites width. In Fig. 2 (d), at $t = 3500$, the $\gamma'$ particle becomes bigger, the order degree becomes higher, and interface width becomes narrower to about 1 site width. It can be also found that two particles are linked by an antiphase domain boundary which is indicated by an arrow.

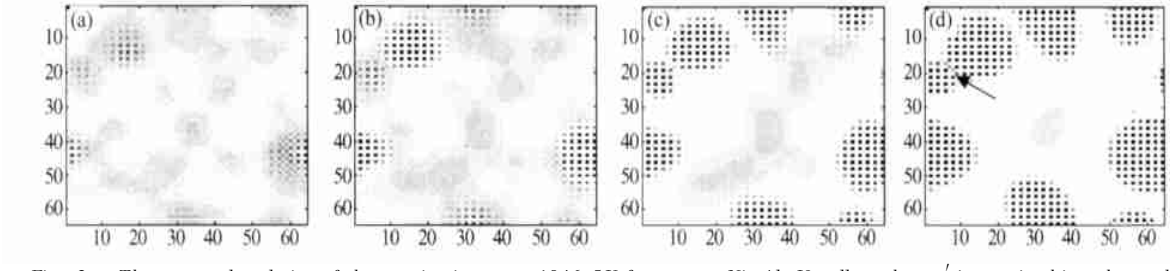


Fig. 2. The temporal evolution of the atomic pictures at 1046.5 K for ternary $Ni_{75}Al_{10}V_{15}$ alloy when $\gamma'$ is a main object observed. (a) $t = 600$; (b) $t = 800$; (c) $t = 1200$; (d) $t = 3500$.

The $\gamma'$ ordered phases obtained in this paper are nearly equiaxed particles, which are different from the cuboidal shape observed in many experimental studies[11 ~ 13]. That is because our work focuses mainly on the very early stage, the interfacial energy plays a dominant role, and the elastic strain energy is relatively small and has been neglected in simulation. So, in order to reduce the interfacial energy and increase the phase transformation driving force, $\gamma'$ grows as spheres. Meanwhile, because the $\gamma'$ phase precipitates very fast, the transient initial spherical shape can hardly be observed in experiment, and usually the cuboidal particles at late stage can be found.

From above atomic pictures, it seems that the $\gamma'$ ordered phase precipitates by a non-classical nucleation mechanism. Yet it is not sufficient to explore the precipitation mechanism only from the phase's morphology. So, we calculated the composition order (c.o) parameters and long range order (l.r.o) parameters of a $\gamma'$ nucleus to discuss its precipitation mechanism further.

The c.o parameter can be obtained by calculating the average value of the occupation probabilities of nine sites including one given site and its eight nearest and sub-nearest lattice sites. The l.r.o parameter of $L1_2$ structure can also be obtained through the following expression:

$$\eta(i,j) = \frac{P(i,j) - C(i,j)}{C(i,j) \times \cos((i+j)\pi)}, \qquad (6)$$

in which $\eta(i,j)$ is the l. r. o parameter of the $(i,j)$ site, $P(i,j)$ the occupation probability of the $(i,j)$ site, $C(i,j)$ is its c. o parameter.

The composition and long-range order parameter profiles across a $\gamma'$ nucleus are plotted in Fig. 3 (a) and (b) respectively. Here $t$ is the time step, which represents the aging time.

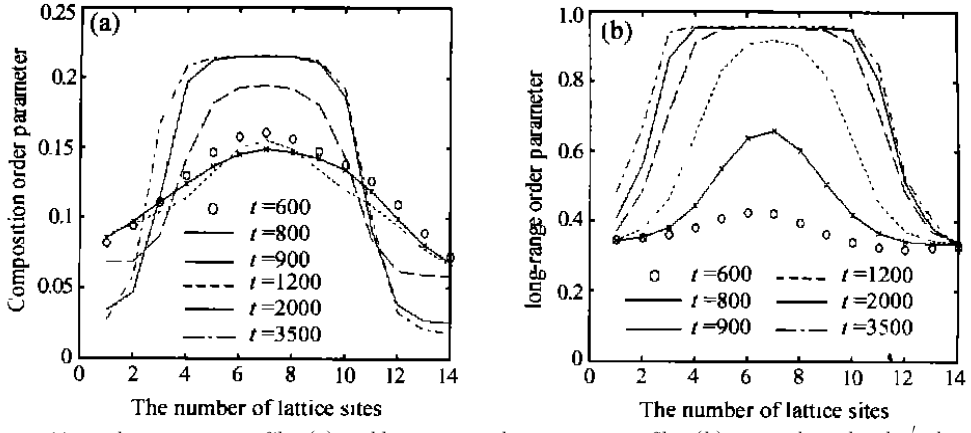


Fig. 3. Composition order parameter profiles (a) and long-range order parameter profiles (b) across the ordered $\gamma'$ phase at different time steps.

In Fig. 3 (a) and (b), it is found that at the same time step, both of the c. o parameters and the l. r. o parameters have the maximum values at the center of a nucleus and the minimum values at the phase boundaries. There is a spatial distance scale in composition and order degree at boundaries, so the interfaces are diffusive. With the increasing aging time, the c. o parameters increase at center and decrease at boundaries, showing that the composition of the new phase becomes higher and higher, and the phase boundaries become narrower and narrower. With the increasing aging time, the l. r. o parameters of centers and boundaries increase simultaneously, showing that the order degree increases in the whole system.

There is an unusual phenomenon that the c. o parameters of the nucleus at center with $t = 600$ are higher than that of the 800th time step. That is because certain noise terms are added to the initial matrix within the earlier 500 time steps to stimulate phase transformation. During this stage, composition fluctuations are higher, so the c. o parameters are higher too. When the noise term is removed, the c. o parameters decrease first and then increase.

At the 600th, 800th and 900th time steps, the two kinds of parameters are lower and do not reach their equilibrium values (0.223 for the composition and 1 for the long-range order parameter). At $t=1200$, the long-range order parameter reaches its equilibrium value, while the composition does not. Therefore the production is nonstoichiometric ordered phase at this time step. Nonstoichiometric $\gamma'$ ordered phase is the $L1_2$ ordered phase whose composition is below that of equilibrium value. It is not a thermodynamic metastable phase. At $t=2000$, both the composition and long-range order parameter reach their equilibrium values, so the stoichiometric ordered phase is formed. In the subsequent stages, the maximum of the composition and long-range order parameter no longer change, but their widths extend, which corresponds to the growth stage of $\gamma'$ phase.

According to the classical nucleation theory, at the center of a new phase nucleus, the composition should reach its equilibrium value, and there is a sudden composition decrease from center to boundary, which is called sharp interface model. In this paper, the new phase nuclei begin with a relatively low composition and do not reach the equilibrium value until the 2000th time step. Moreover, the interfaces between the two phases are diffusive. So, it can be concluded that the $\gamma'$ phase is precipitated by a non-classical nucleation mechanism.

## 2.2 Precipitation behavior of $\theta$ phase

The equilibrium $DO_{22}$ ordered structure diagram, its projection on [001] and its nonstoichiometric one's projection on [001], are shown in Fig. 4 (a) ~ (c). The circle's gray level represents the occupation probability of V atoms, the white is 0 and the black is 1. The sites at the corner and the crossing of the two central lines are defined as B sites, others A sites. In

Fig.4 (b), the finding probabilities of V atoms sitting at B sites are near 1, while sitting at A sites are near 0. In Fig. 4 (c), the finding probabilities of V atoms at B sites are always higher than that at A sites, yet their values may be far lower than 1. We call the ordered phases satisfying this type structure nonstoichiometric ordered phases.

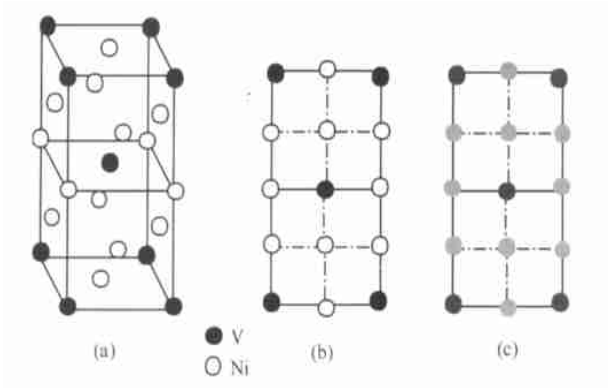


Fig. 4. The snucture of equilibrium $\theta$ phase (a), its projection on [001] orientation (b) and projection of nonstoichiometric $\theta$ ordered phase on [001] orientation (c).

Fig. 5 (a ~ d) shows the morphological evolution of the $Ni_{75}Al_{10}V_{15}$ alloy at different time steps with the $\theta(Ni_3V)$ phase mainly examined.

The simulation results with $t = 600$ are given in Fig. 5 (a). The $\gamma'$ phase already appeared, and near their phase boundaries the occupation probabilities of V atoms are higher. In Fig. 5 (b), at $t = 800$, the V atoms begin to segregate at the $\gamma'$ phase boundaries. In Fig. 5 (c), at $t = 1200$, notice that another ordered phase begins to appear, in which the V atoms are arranged in a hexagonal fashion (it is not truly hexagonal since not all sides have the equal length), consistent with the projection of the $DO_{22}$ structure as shown in Fig. 4. These $DO_{22}$ domains could be the $\theta(Ni_3V)$ phase. In Fig. 5 (d), at $t = 10000$, many $DO_{22}$ domains appear, the occupation probabilities of V atoms at B sites are lower than 1, and the occupation probabilities of V atoms at A sites are heterogeneous, which satisfies the definition of nonstoichiometric ordered phases. So we consider that they could be nonstoichiometric $\theta$ ordered phases.

We also found that $DO_{22}$ ordered domains existed in two orientations in accordance with their adjacent $\gamma'$ phase boundaries: a horizontal one and a vertical one. The farther from the $\gamma'$ phase boundaries, the lower the order degree of $\theta$ domains is. Thus some clusters of V atoms with $DO_{22}$ ordered characteristics are formed in the relatively farther zones.

Poduri explored the reason why the $L1_2$ ordered phase appeared earlier than the $DO_{22}$ ordered phase from the view of thermodynamic driving force[15]. He proposed that the initial disordered matrix should be absolutely unstable with respect to the $L1_2$ phase, and metastable to the $DO_{22}$ phase in $Ni_{75}Al_{10}V_{15}$. The thermodynamic driving force transforming to $L1_2$ phase is stronger than that transforming to $DO_{22}$ phase. So $\gamma'$ phase appeared before $\theta$ domains. Our simulation results are consistent with his study.

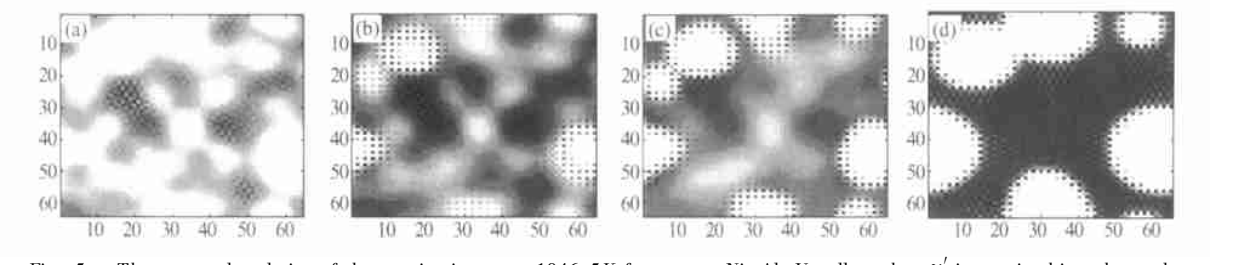


Fig. 5. The temporal evolution of the atomic pictures at 1046.5K for ternary $Ni_{75}Al_{10}V_{15}$ alloy when $\gamma'$ is a main object observed. (a) $t = 600$; (b) $t = 800$; (c) $t = 1200$; (d) $t = 10000$.

Ref. [16] reports that the pseudobinary $Ni_3Al$-$Ni_3V$ might be easily formed when the V element was added to the binary Ni-Al alloy. While in our study, the $Ni_3Al$ phases precipitate by a non-classical nucleation mechanism, yet the $Ni_3V$ just formed with the nonstoichiometric $DO_{22}$ ordered phases. The reason needs to be explored further. We simulated the early precipitation process of $Ni_{75}Al_9V_{16}$, and found its precipitation mechanism was similar to $Ni_{75}Al_{10}V_{15}$. Compared to $Ni_{75}Al_9V_{16}$, the width of interface in $Ni_{75}Al_{10}V_{15}$ is wider, which shows that with the increase in Al atom content, the non-classical nucleation characteristic becomes more obvious.

## 3 Conclusions

In this paper, the extended microscopic diffuse

form of a phase-field model for precipitation process of a ternary system is introduced. The early stage of $Ni_{75}Al_{10}V_{15}$ aged at 1046.5 K was investigated using computer simulations based on this model. Simulation results show that:

(i) Any a priori assumption about a new phase structure and precipitation mechanism is unnecessary; the microscopic diffusion model can describe the atomic ordering, composition clustering, and two ordered phase precipitation simultaneously.

(ii) The $\gamma'$ phases precipitate by a non-classical nucleation mechanism. The sequences are: super saturation solid solution → nonstoichiometric ordered phases→stoichiometric ordered phases→growth.

(iii) After the $\gamma'$ phase has precipitated, the V atoms will segregate at the $\gamma'$ phase boundaries, and gradually transform to the nonstoichiometric $\theta$ ordered phases. The farther is the location from $\gamma'$ phase boundary, the lower the order degree of $\theta$ phase. There exist two kinds of $DO_{22}$ ordered domains: horizontal one and vertical one, which are related to their adjacent $\gamma'$ phase boundaries.

**Acknowledgement** We thank Professor L. Q. Chen (Pennsylvania State University) for giving us many helpful suggestions in our study.

## References

1 Miyazaki, T. Recent developments and the future of computations science on microstructure formation. Material Transactions, 2002, 43 (6): 1266.
2 Chen, L. Q. Phase-field models for microstructure evolution. Annu. Rev. Mater. Res., 2002, 32: 113.
3 Satoshi, H. et al. Short range order and its transformation to long range order in $Ni_4Mo$. Acta Mater., 1998, 46(3): 881.
4 Sabine, D. et al. Fourier analysis of turing-like pattern formation in cellular automaton models. Future Generation Computer Systems, 2001(17): 901.
5 Collins, J. B. et al. Diffuse interface model of diffusion-limited crystal growth. Phys. Rev. B, 1985, 31(9): 6119.
6 Khachaturyan, A. G. Theory of Structural Transformations in Solids. New York: Wiley, 1983, 139.
7 Khachaturyan, A. G. Theory of Structural Transformations in Solids. New York: Wiley, 1983, 129.
8 Chen, L. Q. A computer simulation technique for spinodal decomposition and ordering in ternary systems. Scripta Metallurgica et Materialia, 1993, 29: 683.
9 Chen, L. Q. Computer simulation of spinodal decomposition in ternary systems. Acta Metall. Mater., 1994, 42(10): 3503.
10 Chen, L. Q. et al. Computer simulation of structural transformations during precipitation of an ordered intermetallic phase. Acta Metal Mater., 1991, 39 (11): 2533.
11 Wendt, H. et al. Nucleation and growth of $\gamma'$ precipitates in Ni-14at%Al. Acta Metall., 1983, 31(10): 1649.
12 Jackson, M. P. et al. Determination of the precipitation kinetics of $Ni_3Al$ in the Ni-Al system using DSC. Materials Science and Engineering, 1999, A264: 26.
13 Susumu, O. et al. Simplified energy analysis on the equilibrium shape of coherent $\gamma'$ precipitates in $\gamma$ matrix with a super spherical shape approximation. Intermetallics, 2002, 10: 343.
14 Li, X. L. et al. Computer investigation for critical nucleus criterion of ordered phase. Nonferrous Metals (in Chinese), 2001, 53(3): 49.
15 Poduri, R. et al. Computer simulation of atomic ordering and compositional clustering in the pseudobinary $Ni_3Al$-$Ni_3V$ system. Acta Mater., 1998, 46: 1719.
16 Zapolsky, H. et al. Atom probe analyses and numerical calculation of ternary phase diagram in Ni-Al-V system. Calphad, 2001, 25 (1): 125.